JOURNAL OF MATERIALS SCIENCE **39** (2004) 1899– 1901

Synthesis and characterization of mesoporous iron-doped TiO_2

CHAO WANG, QING LI, RUODING WANG
Shanghai Institute of Ceramics, Chinese Academy of Sciences, 1295 Ding-xi Road, Shanghai 200050, People's Republic of China
E-mail: wangc16890@yahoo.com.cn

Titania is a well-known semiconductor that possesses a high photoactivity [1]. Most ultrafine TiO_2 nanocrystals exhibit high photocatalytic properties, however two main problems occur in practical application. First, ultrafine nanocrystals will agglomerate into larger particles. Second, it is very hard to recover TiO_2 nanocrystals from water [2]. TiO_2 photocatalyst was immobilized for water treatment at the cost of the decrease of photocatalytic activity [3]. Mesoporous TiO_2 can reduce such problems and have still high photocatalytic activity [4–8]. In addition, considerable effort has been devoted to the study of iron-doped TiO_2 and many experiments have demonstrated that TiO_2 with small amount Fe^{3+} doping showed enhanced activity [9–13]. The generally accepted mechanism to explain this improved photocatalytic performance is the formation of shallow charge trapping sites within the TiO_2 matrix as well as on the particles' surface through the replacement of Ti^{4+} by Fe^{3+} [10]. Thus, the undesirable recombination of electron/hole pairs can be partially prevented.

Ionic and neutral surfactants have been successfully employed as templates to prepare mesoporous TiO_2 [14–16]. Block copolymer can also be used as a template to direct the formation of mesoporous TiO_2 [17]. In addition, many nonsurfactant organic compounds have been used as poreformers [18, 19]. Here, we report a simple method to prepare mesoporous iron-doped TiO_2 by using glycerin as a pore-forming agent via sol-gel and hydrothermal processes. Before calcination, hydrothermal treatment is applied to crystallize amorphous TiO_2 into anatase and stabilize mesoporous structure, which result in powders with a high thermal stability up to 773 K.

Mesoporous iron-doped TiO_2 was prepared as follows. After 50 ml tetrabutyl orthotitanate was dissolved in 126 ml ethanol, 3 ml acetylaceton was added with continuous stirring for 30 min. Then 6.2 ml of 4.76 M HNO_3 was added dropwise into the above solution with stirring for 1 h at room temperature. Next, $Fe(NO_3)_3{\cdot}9H_2O$ was added according to the required iron dopant amounts: Fe/Ti = 0, 1, 2, 3, 4, 5 at.% (leading to samples denoted TF0, TF1, TF2, TF3, TF4, TF5, respectively). Finally, 6.3 ml glycerin was added with stirring for 1 h at room temperature. After gelation, the aerogel was dried at 363 K for 12 h, ground and sieved to a particle size finer than 100 μm. Then 4 g xerogel powders suspended in 15 ml distilled water were put into an autoclave for hydrothermal treatment at 393 K for 24 h. Crystalline powders were recovered by filtration, washed with water and ethanol, dried at 383 K overnight. In order to eliminate organic materials and improve crystallinity, the recovered powders were calcined at 673, 773, and 873 K for 2 h, respectively. Transmission electron microscopy (TEM) images were obtained on a Jeol-200CX electron microscope. Nitrogen adsorption data were collected on a Micromeritics ASAP 2010 nitrogen adsorption apparatus. X-ray diffraction (XRD) patterns were obtained on an automated D/max 2550 v. The diffuse reflectance spectra of the samples were performed on Shimadzu UV-3101 PC spectrophotometer.

HNO_3-catalyzed sol-gel processes proceeded in the presence of glycerin. The higher the glycerin content, the less time was needed for gelation. Acetylaceton had to be added as a stabilizer in order to prevent the sol from becoming opaque. The glycerin content had a small effect on the pore parameters. Fig. 1 depicts XRD patterns of the powders. TiO_2 xerogel was amorphous (Fig. 1a). After hydrothermal treatment, the broad anatase peaks appeared (Fig. 1b). After TF0 were calcined at 673 K for 2 h, the intensity of the anatase peaks became stronger (Fig. 1c), indicating that larger size particles were formed.

The type IV N_2 adsorption-desorption isotherms in Fig. 2 clearly illustrate the mesoporous nature of TF5 calcined at 673 K for 2 h, while the H2 hysteresis between the two curves indicates that there is a diffusion bottleneck. The inserted pore size distribution shows a

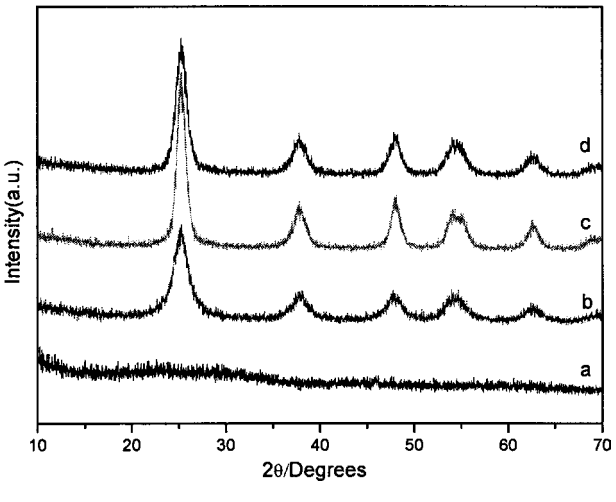

Figure 1 XRD patterns of (a) TiO_2 xerogel, (b) TiO_2 xerogel after hydrothermal treatment, (c) TF0 calcined at 673 K for 2 h and (d) TF5 calcined at 673 K for 2 h.

TABLE I Physicochemical properties of mesoporous iron-doped TiO_2 at various calcination temperatures

Sample	TF0	TF1	TF2	TF3	TF4	TF5	TF5	TF5
Temperature (K)	673	673	673	673	673	673	773	873
Surface area ($m^2.g^{-1}$)	139.6	165.8	165.2	165.0	180.2	190.2	114.9	25.8
Pore volume ($cm^3.g^{-1}$)	0.17	0.29	0.27	0.30	0.32	0.33	0.22	0.06
Average pore diameter (nm)	4.7	6.8	6.3	6.8	6.7	6.7	7.3	8.5

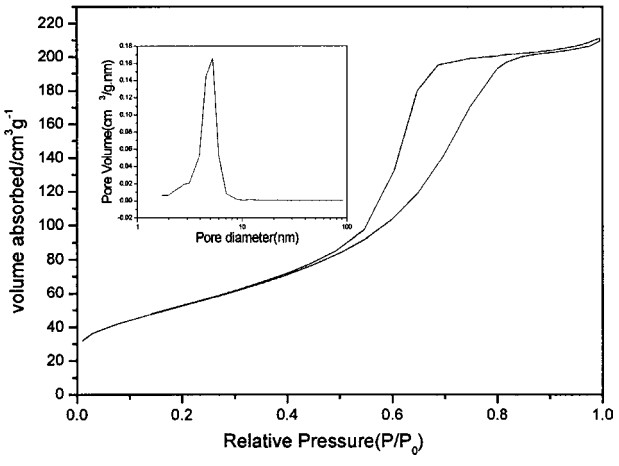

Figure 2 N_2 adsorption-desorption isotherm and BJH pore size distribution plot (inset) of TF5 calcined at 673 K for 2 h.

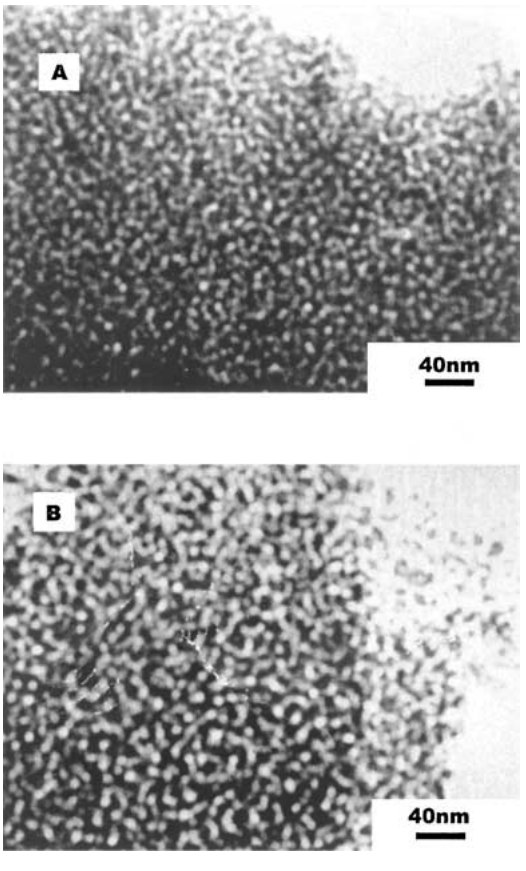

Figure 3 TEM images of (A) TF0 and (B) TF5 calcined at 673 K for 2 h.

narrow range of 2–10 nm with an average pore diameter of 7 nm. Fig. 3A and B show TEM images of TF0 and TF5 calcined at 673 K for 2 h respectively. TEM images reveal that wormhole-like pores appear throughout the aggregates. The corresponding pore sizes are consistent with average pore diameters listed in Table I.

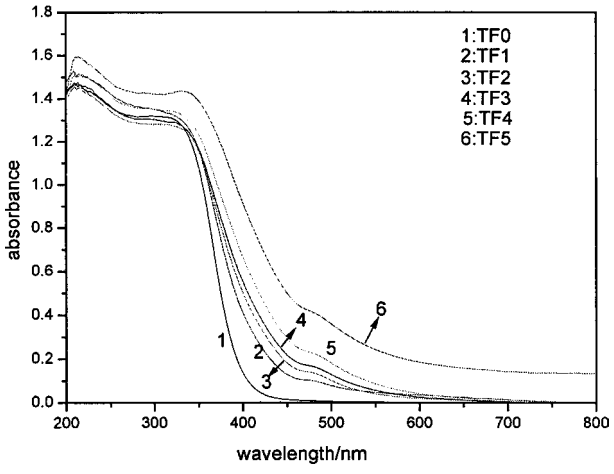

Figure 4 UV-absorption spectra of TF0-TF5 calcined at 673 K for 2 h.

The physicochemical properties of the samples with 40 wt% glycerin content are reported in Table I. As shown by the data for TF5 with the increase of calcination temperature, the surface area and pore volume all become smaller and the pore diameter increases because micropores collapse. At 673 K, the surface area of iron-doped TiO_2 is always higher than that of TF0. This is ascribed to the fact that Fe(III) has a retarding effect on TiO_2 anatase crystallites growth, which will favor the formation of smaller TiO_2 crystallites [20]. It is confirmed by XRD patterns of Fig. 1c and d. According to Scherrer equation, the average crystallite size of TF0, TF5 is 14 nm, 13 nm, respectively.

After TF5 xerogel powders without hydrothermal treatment were calcined at 673 K for 2 h, the obtained powders had the surface area as low as 36 m^2/g. However, After TF5 xerogel powders with hydrothermal treatment were calcined at 773 K for 2 h, the obtained powders still had the surface area as high as 114 m^2/g. Hydrothermal treatment increases the thermal stability of the powders significantly. This may be explained as follows. Generally, mesopores collapse during calcining process due to the crystallization of the wall from amorphous phase to anatase. After hydrothermal treatment induced the crystallization of amorphous xerogel powders, the obtained crystalline powders can effectively sustain the local strain caused by the crystallization during calcining process and prevent the mesopores from collapsing.

Fig. 4 shows UV absorption spectra of selected samples with various iron contents. It can be seen that the absorption range is progressively broadened to the visible region when the iron content increases. Absorption in the visible region may make photocatalysts utilize sunlight more effectively in some photocatalytic reactions.

In summary, mesoporous iron-doped TiO_2 with high thermal stability and high surface area was prepared by a novel gel-hydrothermal route. Hydrothermal treatment increases the thermal stability of the powders significantly. It has also been found that the UV-absorption range of mesoporous TiO_2 can be broadened to the visible region by iron doping. These mesoporous materials with anatase wall can be applied promisingly in visible light-activated photocatalysis.

References

1. M. HOFFMANN, S. MARTIN, W. CHOI and D. BAHNEMANN, *Chem. Rev.* **95** (1995) 69.
2. D. BEYDOUN, R. AMAL, G. K.-C. LOW and S. MCEVOY, *J. Phys. Chem.* **104** (2000) 4387.
3. J.-M. HERRMANN, H. TAHIRI, Y. AIT-ICHOU, G. LASSALETTA, A. R. GONZALES-ELIPE and A. FERNANDEZ, *Appl. Catal.* B. **13** (1997) 219.
4. J. C. YU, L. Z. ZHANG and J. G. YU, *Chem. Mater.* **14** (2002) 4647.
5. H. Y. ZHU, J. A. ORTHMAN, J.-Y. LI, J.-C. ZHAO, G. J. CHURCHMAN and E. F. VANSANT, *ibid.* **14** (2002) 5037.
6. Q. H. ZHANG, L. GAO and S. ZHENG, *Chem. Lett.* **11** (2001) 1124.
7. Q. DAI, N. Y. HE, Y. GUO and C. W. YUAN, *ibid.* **11** (1998) 1113.
8. J. C. YU, J. G. YU, W. K. HO, Z. T. JIANG and L. Z. ZHANG, *Chem. Mater.* **14** (2002) 3808.
9. W. CHOI, A. TERMIN and M. R. HOFFMANN, *J. Phys. Chem.* **98** (1994) 13669.
10. M. I. LITTER and J. A. NAVIO, *J. Photochem. Photobiol. A: Chem.* **98** (1996) 171.
11. C. Y. WANG, D. W. BAHNEMANN and J. K. DOHRMANN, *Chem. Commun.* (2000) 1539.
12. M. GRAETZEL and R. F. HOWE, *J. Phys. Chem.* **94** (1990) 2566.
13. J. SORIA, J. C. CONESA, V. AUGUGLIARO, L. PALMISANO, M. SCHIAVELLO and A. SCLAFANI, *ibid.* **95** (1991) 274.
14. R. L. PUTNAM, N. NAKAGAWA, K. M. MCGRATH, N. YAO, I. A. AKSAY, S. M. GRUNER and A. NAVROYSKY, *Chem. Mater.* **9** (1997) 2690.
15. V. F. STONE JR. and R. J. DAVIS, *ibid.* **10** (1998) 1468.
16. M. THIEME and F. SCHUTH, *Micropor. Mesopor. Mater.* **27** (1999) 193.
17. P. D. YANG, D. Y. ZHAO, D. I. MARGOLESE, B. F. CHMELKA and G. D. STUCKY, *Nature* **396** (1998) 152.
18. J. Y. ZHENG, J. B. PANG, K. Y. QIU and Y. WEI, *Micropor. Mesopor. Mater.* **49** (2001) 189.
19. J. Y. ZHENG, K. Y. QIU and Y. WEI, *Mol. Cryst. Liq. Cryst.* **354** (2000) 183.
20. Y. H. ZHANG and A. RELLER, *J. Mater. Chem.* **11** (2001) 2537.

Received 19 June
and accepted 16 September 2003